Tunable structures comprising two photonic crystal slabs – optical study in view of multi-analyte enhanced detection

Lina Shi, Pierre Pottier, Maksim Skorobogatiy and Yves-Alain Peter

Engineering Physics Department, Ecole Polytechnique de Montréal,
Montréal (QC) H3C 3A7, Canada

yves-alain.peter@polymtl.ca

Abstract: Using finite-difference time-domain method, we characterize the normal-incidence transmission properties of a two slab photonic crystal device in a view of its applications in fluorescence enhancement and multi-analyte detection. Individual slabs consist of a square or a triangular lattice of air holes embedded into a silicon nitride slab. The geometrical parameters are chosen so that the individual slabs operate in a guided resonance regime where strong reflectivity under the normal incidence angle is observed in a broad spectral range. When placed in the close proximity of each other, the two photonic crystal slab system exhibits a narrow Fabry-Perot type transmission peak corresponding to the excitation of a resonant mode in the cavity formed by the two slabs. We then study the effects of the size of the air gap between the two photonic crystal slabs on the spectral position and bandwidth of a resonance transmission peak. Finally, we investigate the electromagnetic energy distributions at the wavelength of a transmission resonance in the double slab photonic crystals. As a final result we demonstrate that this structure can provide electric field enhancement at the slab surface, which can be used for fluorescence enhancement.

© 2009 Optical Society of America

OCIS codes: (230.5298) Photonic crystals; (260.5740) Resonance; (260.2510) Fluorescence; (230.3990) Micro-optical devices.

References and links

1. A. Miyawaki, "Visualization of the spatial and temporal dynamics of intracellular signaling," Dev. Cell **4**, 295 (2003).
2. T. Chishima, Y. Miyagi, X. Wang, H. Yamaoka, H. Shimada, A. R. Moossa, and R. M. Hoffman, "Cancer Invasion and Micrometastasis Visualized in Live Tissue by Green Fluorescent Protein Expression," Cancer Res. **57**, 2042 (1997).
3. P. C. Mathias, N. Ganesh, L. L. Chan, and B. T. Cunningham, "Combined enhanced fluorescence and label-free biomolecular detection with a photonic crystal surface," Appl. Opt. **46**, 2351 (2007).
4. N. Ganesh, W. Zhang, P. C. Mathias, E. Chow, J. A. N. T. Soares, V. Malyarchuk, A. D. Smith, and B. T. Cunningham, "Enhanced fluorescence emission from quantum dots on a photonic crystal surface," Nature Nanotech. **2**, 515 (2007).
5. P. C. Mathias, N. Ganesh, W. Zhang, and B. T. Cunningham, "Graded wavelength one-dimensional photonic crystal reveals spectral characteristics of enhanced fluorescence," J. Appl. Phys. **103**, 094320 (2008).
6. N. Ganesh, P. C. Mathias, W. Zhang, and B. T. Cunningham, "Distance dependence of fluorescence enhancement from photonic crystal surfaces," J. Appl. Phys. **103**, 083104 (2008).
7. Y. Kanamori, T. Kitani, and K. Hane, "Control of guided resonance in a photonic crystal slab using microelectromechanical actuators," Appl. Phy. Lett. **90**, 031911 (2007).

8. W. Suh, M. F. Yanik, O. Solgaard, and S. Fan, "Displacement-sensitive photonic crystal structures based on guided resonance in photonic crystal slabs," Appl. Phy. Lett. **82**, 1999 (2003).

9. W. Suh, O. Solgaard, and S. Fan, "Displacement sensing using evanescent tunneling between guidedresonances in photonic crystal slabs," J. Appl. Phys. **98**, 033102 (2005).

10. R. Magnusson, and S. S. Wang, "New principle for optical filters," Appl. Phys. Lett. **61**, 1022-1024 (1992).

11. S. Peng, and G. M. Morris, "Resonant scattering from two-dimensional gratings," J. Opt. Soc. Am. A **13**, 993-1005 (1996).

12. M. Kanskar, P. Paddon, V. Pacradouni, R. Morin, A. Busch, J. F. Young, S. R. Johnson, J. MacKenzie, and T. Tiedje, "Observation of leaky slab modes in an air-bridged semiconductor waveguide with a two-dimensional photonic lattice," Appl. Phys. Lett. **70**, 1438-1440 (1997).

13. M. Boroditsky, R. Vrijen, T. F. Krauss, R. Coccioli, R. Bhat, and E. Yablonovitch, "Spontaneous emission extraction and Purcell enhancement from thin-film 2-D photonic crystals," J. Lightwave Technol. **17**, 2096-2112 (1999).

14. V. N. Astratov, I. S. Culshaw, R. M. Stevenson, D. M. Whittaker, M. S. Skolnick, T. F. Krauss, and R. M. De la Rue, "Resonant coupling of near-infrared radiation to photonic band structure waveguides," J. Lightwave Technol. **17**, 2050-2057 (1999).

15. V. Pacradouni, W. J. Mandeville, A. R. Cowan, P. Paddon, and J. F. Young, "Photonic band structure of dielectric membranes periodically textured in two dimensions," Phys. Rev. B, **62**, 4204-4206 (2000).

16. A. R. Cowan, P. Paddon, V. Pacradouni, and J. F. Young, "Resonant scattering and mode coupling in two dimensional textured planar waveguides," J. Opt. Soc. Am. A **18**, 1160-1170 (2001).

17. S. Fan, and J. D. Joannopoulos, "Analysis of guided resonances in photonic crystal slabs," Phys. Rev. B **65**, 235112 (2002).

18. M. Szekeres, O. Kamalin, R. A. Schoonheydt, K Wostyn, K. Clays, A. Persoonsc, and I. Dékány, "Ordering and optical properties of monolayers and multilayers of silica spheres deposited by the Langmuir Blodgett method," J. Mater. Chem. **12**, 3268-3274 (2002).

19. O. Kilic, S. Kim, W. Suh, Y.-A. Peter, A. S. Sudbø, M. F. Yanik, S. Fan, and O. Solgaard, "Photonic crystal slabs demonstrating strong broadband suppression of transmission in the presence of disorders," Opt. Lett. **29**, 2782-2784 (2004).

20. V. Lousse, W. Suh, O. Kilic, S. Kim, O. Solgaard, and S. Fan, "Angular and polarization properties of a photonic crystal slab mirror," Opt. Express **12**, 1575-1582 (2004).

21. L. Landström, D. Brodoceanu, N. Arnold, K. Piglmayer, and D. Bäuerle, "Photonic properties of silicon-coated colloidal monolayers," Appl. Phys. A **81**, 911-913 (2005).

22. A. Rosenberg, M. W. Carter, J. A. Casey, M. Kim, R. T. Holm, R. L. Henry, C. R. Eddy, V. A. Shamamian, and K. Bussmann, "Guided resonances in asymmetrical GaN photonic crystal slabs observed in the visible spectrum," Opt. Express **13**, 6564-6571 (2005).

23. K. B. Crozier, V. Lousse, O. Kilic, S. Fan, and O. Solgaard, "Air-bridged photonic crystal slabs at visible and near-infrared wavelengths," Phys. Rev. B **73**, 115126 (2006).

24. Z. Jian and D. M. Mittlemana, "Characterization of guided resonances in photonic crystal slabs using terahertz time-domain spectroscopy," J. Appl. Phys. **100**, 123113-123118 (2006).

25. T. Prasad, V. L. Colvin, and D. M. Mittleman, "The effect of structural disorder on guided resonances in photonic crystal slabs studied with terahertz time-domain spectroscopy," Opt. Express **15**, 16954-16965 (2007).

26. J. L. Skinner, A. A. Talin, and D. A. Horsley, "A MEMS light modulator based on diffractive nanohole gratings," Opt. Express **16**, 3701-3711 (2008).

27. L. Prodan, R. Hagen, P. Gross, R. Arts, R. Beigang, C. Fallnich, A. Schirmacher, L. Kuipers, and K-J Boller,"Mid-IR transmission of a large-area 2D silicon photonic crystal slab," J. Phys. D: Appl. Phys. **41**, 135105-135111 (2008).

28. Y. Nazirizadeh, J. G. Mller, U. Geyer, D. Schelle, E. Kley, A. Tünnermann, U. Lemmer, and M. Gerken, "Optical characterization of photonic crystal slabs using orthogonally oriented polarization filters," Opt. Express **16**, 7153-7160 (2008).

29. G. Alagappan, X. W. Sun, and M. B. Yu, "Out-of-plane diffraction of a two-dimenisonal photonic crystal with finite dielectric modulation," J. Opt. Soc. Am. A **25**, 1098-1103 (2008).

30. S. G. Johnson, "Meep", http://ab-initio.mit.edu/wiki/index.php/Meep.

31. E. M. Purcell, "Spontaneous emission probabilities at radio frequencies," Phys. Rev. **69**, 681 (1946).

32. W. L. Barnes, G. Bjork, J. M. Gerard, P. Jonsson, J. A. E. Wasey, P. T. Worthing, and V. Zwiller, "Solid-state single photon sources: light collection strategies," Eur. Phys. J. D **18**, 197-210 (2002).

33. J. M. Gerard, B. Sermage, B. Gayral, B. Legrand, E. Costard, and V. Thierry-Mieg, "Enhanced Spontaneous Emission by Quantum Boxes in a Monolithic Optical Microcavity," Phys. Rev. Lett. **81**, 1110-1113 (1998).

34. D. Englund, D. Fattal, E. Waks, G. Solomon, B. Zhang, T. Nakaoka, Y. Arakawa, Y. Yamamoto, and J. Vučković, "Controlling the spontaneous emission rate of single quantum dots in a two-dimensional photonic crystal," Phys. Rev. Lett. **95**, 013904-1–013904-4 (2005).

1. Introduction

Fluorescence is important to both in-vivo cellular imaging and in-vitro assay detection.[1,2] The importance of fluorescence-based detection methods has motivated engineering of optically active structures capable of enhancing the fluorescent signal. Photonic crystal (PhC) slabs have demonstrated the capability to enhance fluorescence due to a combination of high-intensity near fields and strong coherent scattering effects of guided resonance.[3–6]

Multi-analyte detection of different pathogens needs different fluorescent labels having different emission wavelengths. In order to realize multi-analyte detection, one should, thus, enhance fluorescence at several distinct wavelengths corresponding to the emission wavelengths of the fluorescent labels under consideration. Moreover, sensing systems for the detection of common diseases are in great need of miniaturization and low cost fabrication processes to be suited for point of care diagnostics. To this end, Mathias et al.[5] have fabricated a PhC with a graded thickness TiO_2 layer which contains reflective resonant peaks for a range of position-dependent wavelengths spanning 100 nm. Ganesh et al.[6] have also shown that the device can be used to excite a broad range of resonant wavelengths by controlling the launching angle.

With a goal of miniaturization of the multi-analyte detection systems, in this paper we report a structure based on a two PhC slab geometry that can enhance the fluorescence signal from quantum dots (QDs) emitting at several distinct wavelengths. Their excitation, their emission, or possibly both in the same time can be enhanced. The structure operates using a narrow-band Fabry-Perot resonance mode confined between the two PhC slabs which operate in the broadband guided resonance regime. Spectral position of a Fabry-Perot resonance can be tuned by changing the gap between the two PhC slabs with a micro electro-mechanical (MEMS) actuator.[7–9] To our knowledge, spectral dependence of the resonance peaks and the field enhancement at the peak wavelength as a function of the structural parameters of a two slab PhC structure have not been investigated in details up to date.

There are many theoretical and experimental studies about guided-mode resonances in PhC slabs.[10–29] In general, one distinguishes two types of guided resonances. The first type of guided resonance can be readily observed in a single PhC slab geometry as a narrow Fano type[17] resonance in transmission and/or reflection spectrum. The second type of guided resonance that can be observed in a single PhC slab geometry is the one which is characterized by the strong reflectivity over a wide spectral range.[7–9] In this paper we are mostly interested in the guided resonances of the second type as structures operating at such resonances can be used as efficient mirrors for the construction of tunable resonant cavities.

In this paper we perform extensive numerical study of the single and double PhC slabs in order to elucidate dependence of the spectral structure of the guided resonances and Fabry-Perot resonances on the parameters of the PhC slabs. In our studies, we first vary the radius of the holes and the thickness of a PhC slab with a goal of finding slab geometries that exhibit broadband reflection. Strong reflectivity of the individual slabs is absolutely necessary for their further application as mirrors in the optical cavity. Particularly, in a double slab configuration, two slabs operating individually in the regime of guided resonance are used as high quality mirrors that confine a Fabry-Perot like mode (sensing mode) inside a gap between the slabs. The Fabry-Perot transmission peaks are highly sensitive to the size of the gap between the two slabs. Therefore, the peak position can be tuned to span a certain spectral range where fluorescence detection is desired. In the remainder of the paper we, therefore, investigate numerically the optimal double slab designs in the context of broadband tunability of the Fabry-Perot mode and optimization of the field enhancement effects.

Our paper is structured as follows. Model and simulation method are introduced in section 2. Section 3.1 focuses on a single slab reflection spectrum. Section 3.2 focuses on tuning the positions of transmission peaks in the two PhC-slab geometry. Section 3.3 is devoted to the res-
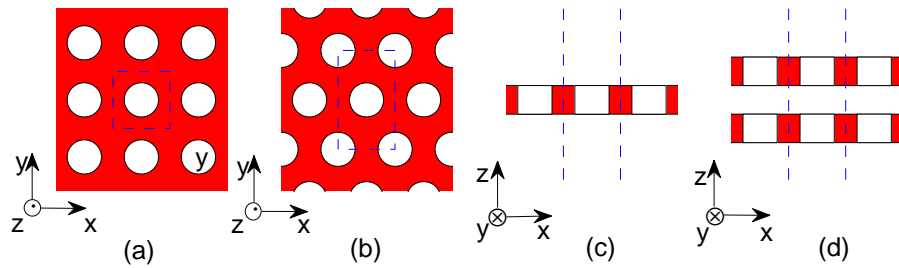
Fig. 1. Schematics of the two PhC lattices used in simulations. The area surrounded by blue dash line denotes the computation domain (unit cell). Top view of the (a) square, and (b) triangular PhC lattices. *xz* cross sections through the middle of the units cells of the (c) single slab, and (d) double slab geometries.

onance energy distribution at the wavelength of a Fabry-Perot transmission peak. A conclusion is presented in section 4.

2. Simulation method and model

Our model system consists of a square (Fig. 1(a)) or a triangular (Fig. 1(b)) lattice of air holes introduced into a silicon nitride slab. Figure 1 shows the computational domain (the area surrounded by blue dash line) that was used in simulations of the normal incidence reflection and transmission spectra. The red regions denotes silicon nitride with refractive index 2.05. The rest (white regions) is air (index 1). The hole radius, the lattice constant, the slab thickness and the gap between the two layers are defined respectively as r, a, t and g.

Our simulations are performed using the Meep implementation of the finite-difference time-domain (FDTD) method.[30] The computation domain includes a single unit cell of the crystal. On the cell surfaces which are perpendicular to the z direction, we impose the Perfectly Matched Layer (PML) absorbing boundary conditions. At the remaining four surfaces, we impose Bloch periodic boundary conditions. The structures are excited by a temporal Gaussian pulse source spanning the frequencies of interest. Spatially, excitation is a plane wave propagating along the z direction. The electric field of the source is polarized along the y direction. In our simulations we use the normalized frequency a/λ, where λ is the light wavelength. In order to get the normal-incidence reflection coefficient (the reflected flux divided by the incident flux), we perform two simulations, one with and another without the PhC slab (for the details of the method see the Meep manual[30]).

3. Simulations and discussion

3.1. Reflection spectra of a single photonic crystal slab

We begin our consideration by calculating the reflection spectra for a variety of single slab geometries by varying the hole radius and slab thickness. Our goal is to find the geometries of single slabs that exhibit strong broadband reflectivity when operating in the regime of guided resonance excitation. Our simulations proceed as follows. For a given hole radius $r = 0.1a$, $0.2a$, $0.3a$, $0.35a$, $0.4a$, $0.45a$, the reflection spectra of the PhC slabs are calculated for ten values of the slab thicknesses $t = 0.1a, 0.2a, ..., 1.0a$ for both the square and triangular lattices. In Fig. 2 we only present the reflection spectra of structures that show strong reflectivities (reflection coefficient larger than 0.5) over wide frequency ranges.
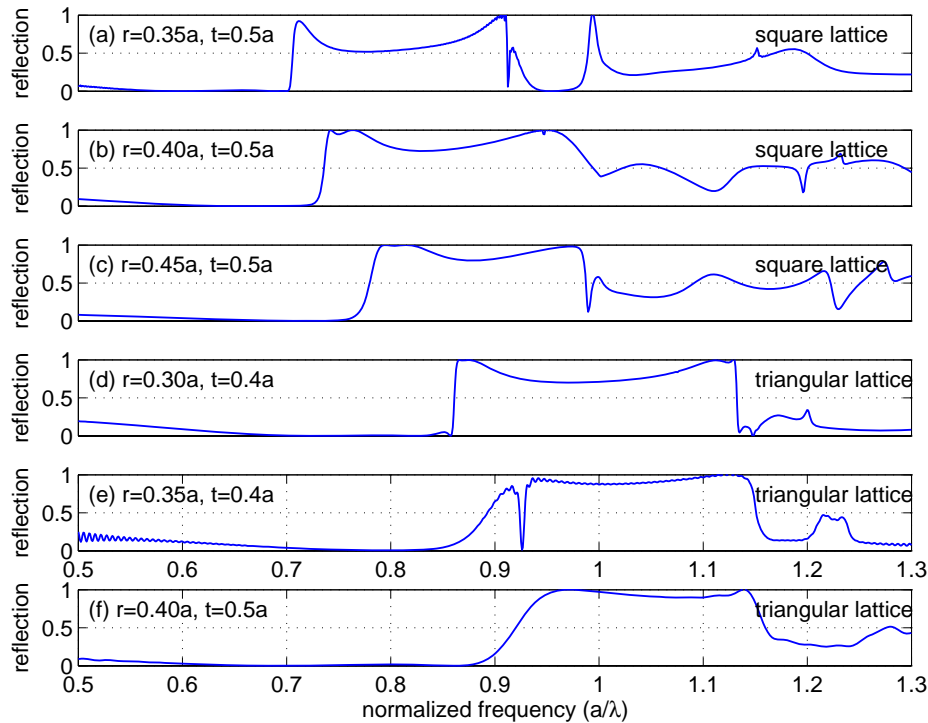
Fig. 2. Reflection spectra of selected single PhC slab structures having strong broadband reflectivities.

An overall conclusion drawn from these simulations is that larger hole sizes promote broader guided resonances, in other words, wider spectral regions of strong reflection. This conclusion agrees well with the existing literature.[17,23] As an example, consider the case of structure (e) in Fig. 2: the reflection spectrum for this PhC slab shows a 100 nm-broad guided resonance centered at 550 nm for $a = 565$ nm. Over the whole bandwidth of this resonance the slab reflectivity is greater than 87%. In what follows we consider in greater details the six highly reflective slabs presented in Fig. 2.

3.2. Tunability of a transmission peak in the two PhC slab geometry

We now investigate transmission properties of the six structures each consisting of the pairs of highly reflective PhC slabs presented in the previous subsection. Figure 3 shows normal incidence transmission spectra of the two slab PhCs as a function of the size of the gap between the slabs. All the transmission spectra exhibit a number of important features. (i) A resonant transmission peak (Fabry-Perot resonance) appears within the high reflectivity spectral region of an individual slab. The transmission peak shifts towards smaller normalized frequencies as the gap size between the two slabs increases. By changing the gap size between two PhC slabs, one can, therefore, select a particular wavelength for further analysis, while still profiting from the field enhancement from the resonant cavity. (ii) The width of the transmission peak depends strongly on the reflectivity of an individual slab. Particularly, the transmission peak is narrower for the slabs with higher reflectivity. As an example consider a particular value of the gap size $g = 1.2a$. From Fig. 3(a), (b) and (c) one can determine that the widths of the Fabry-Perot transmission peaks are, respectively, 0.0348, 0.0157, 0.0090 in normalized frequency, while
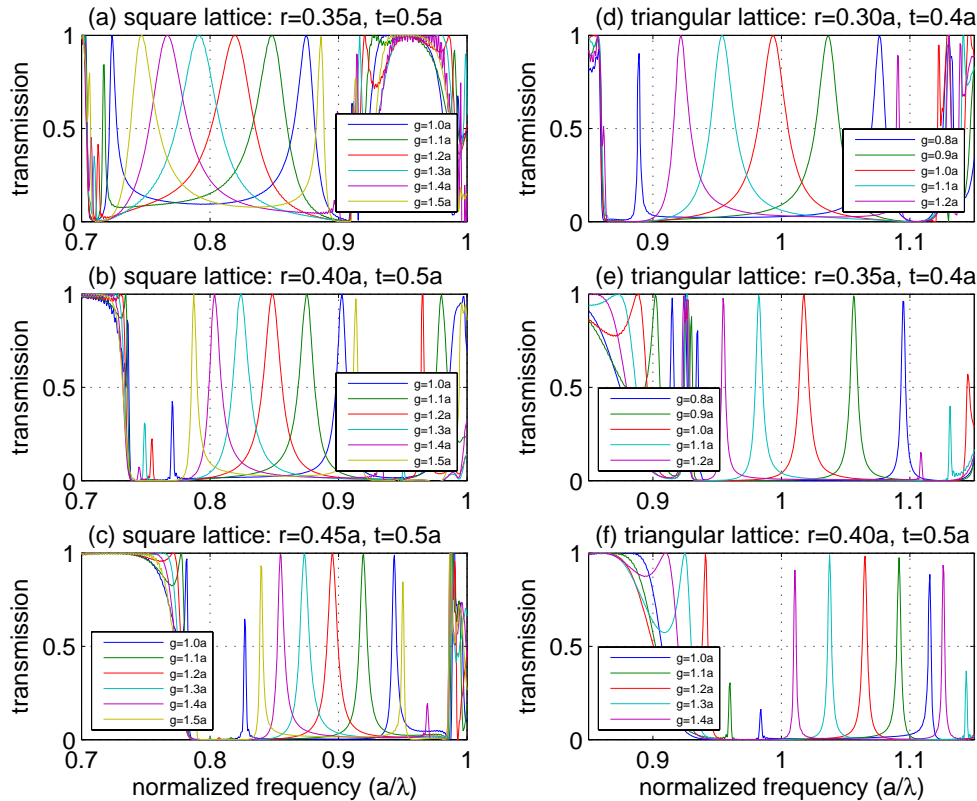
Fig. 3. Transmission spectra of the two slab PhCs. Different colors denote different sizes of the gap *g* separating the two slabs. (a), (b) and (c) are for the square lattice PhCs. (d), (e) and (f) are for the triangular lattice PhCs.

the corresponding slab reflectivities are 0.55, 0.73, 0.81.

The above mentioned observations are trivial to rationalize if we consider the two slab PhCs as two broadband mirrors creating a Fabry-Perot cavity supporting a resonant mode. To justify this assumption, in Fig. 4(a-f) we present the electromagnetic field energy distributions in the Fabry-Perot cavity modes ($g = 1.2a$ or $g = 1.0a$) with the following normalized frequencies $f_n = 0.8198, 0.8486, 0.8955, 0.9937, 1.018, 1.065$. Individual energy distributions are presented in the *xz* plane and are calculated using plane wave source with the fixed frequency corresponding to the frequency of a resonance under consideration. By observing the energy distributions versus time one can clearly identify a standing wave excitation positioned between the two slabs, thus confirming that such slabs effectively act as mirrors, while forming a Fabry-Perot cavity that supports a resonant mode.

3.3. *Energy distribution and enhancement of optical field intensity at the slab surface*

In order to obtain the fluorescence enhancement from the QDs or other fluorescent labels that could be, potentially, deposited on the PhC surface, one needs to enhance the electric field intensity at the interface of a PhC slab. To qualify the field enhancement effects in a two slab PhC structure we compute the time averaged linear density of the electromagnetic field energy. For a given value of a *z* coordinate, such a density is computed by integrating the local volumic density of energy over the *xy* plane of an elementary lattice cell, and then averaging such a
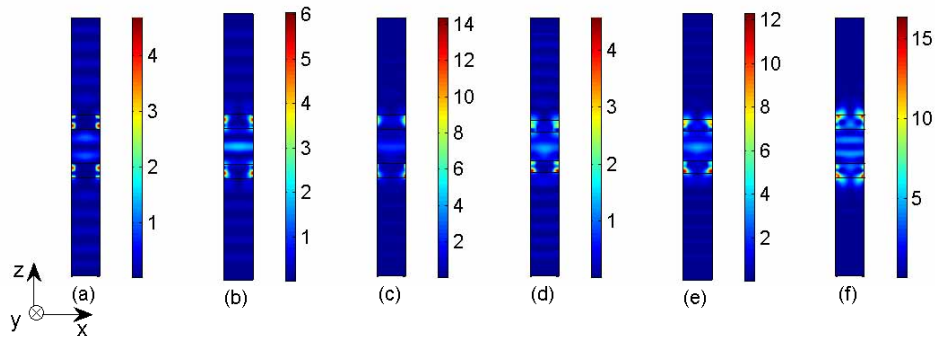
Fig. 4. Snapshots of the electromagnetic field energy distributions across the xz plane of a unit cell. Individual distributions are calculated using a CW plane wave excitation source with a frequency corresponding to the frequencies of respective transmission resonances (red curves) in Figs. 3(a-f), $g = 1.2a$ or $g = 1.0a$.

quantity over one time period. The linear energy densities in z direction are plotted in Fig. 5 versus z: electric energy (red lines), magnetic energy (green lines) and total energy (blue lines). The yellow areas represent regions occupied by the PhC slabs. Figures 5(a-f) correspond to the respective red transmission peaks in Fig. 3(a-f), $g = 1.2a$ or $g = 1.0a$. The linear energy density of an incident wave is taken as 1.

As seen from Fig. 5 the maximum linear electric energy density is found inside the slab and in the close vicinity of the external air/slab interface. From Fig. 5 we summarize that at this interface, on the air side, the enhancement of the electric field intensity relative to its value in free space is respectively 2.46, 6.25, 14.0, 5.08, 16.0, 32.3 for cases (a-f). Because the Meep algorithm uses index smoothing at the interface, we used a polynomial extrapolation (7th degree) of the field evolution on the air side to the exact interface location for a precise determination of it.

An interesting point to note is that, contrary to a classical Fabry-Perot cavity composed of Bragg mirrors where the electric energy density is maximum in the gap and decreases in the distributed mirrors, we have here a maximum in the mirror, and close to the external air/slab interface. This is of great interest for biological sample testing where QDs can be in front of the medium to detect (wet), which is easily brought by microfluidics system, while the rest of the optical MEMS stays in a dry separated environment, provided that a thin layer of isolation is placed in between. By example, a $0.05a - 0.10a$ thick SiO_2 layer (refractive index 1.45) could be used. For the structure of Fig. 5(c) and the operating wavelength $\lambda = 550$ nm (normalized frequency 0.88, red peak in Fig. 3(c)), this layer thickness would be $24.2 - 48.4$ nm. This isolation layer affects the resonances, but only by shifting the transmission peaks which is not a problem for our device, and keeps the same shape of peaks as without the layer (Fig. 6(a)). The electric field intensity enhancement at the air/slab interface (Fig. 6(b) and (c)) even remains the same as in Fig. 5(c).

To further discuss this point of energy localization, we calculated the different ratios of energy at the surface to the energy in the gap and plotted them versus the quality factor (Fig. 7(a)). First we can see that these ratios vary from one structure to the other, and second we can observe a general trend of increase with the quality factor. The electric field intensity enhancement can then potentially still be increased, by an adequate adjustment of the design of the two
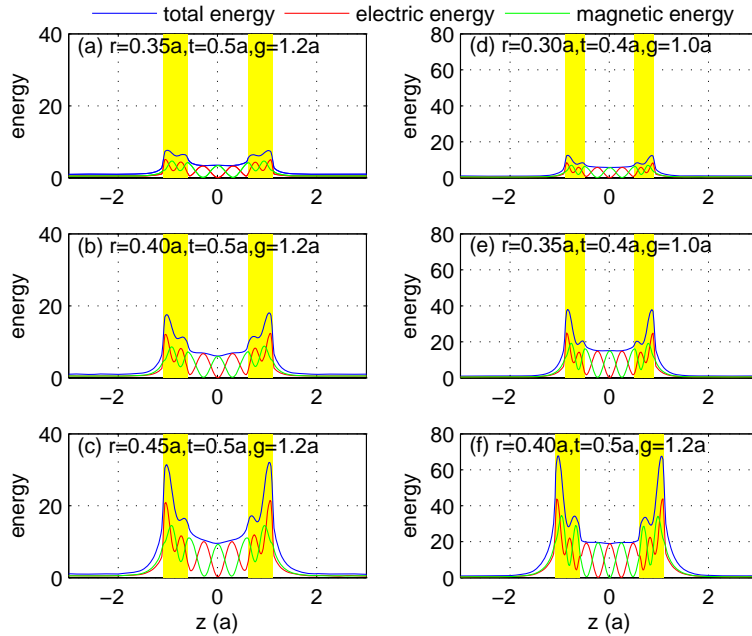
Fig. 5. Time averaged linear density of the electric energy (red lines), magnetic energy (green lines) and total energy (blue lines) along the z direction. The yellow areas denote positions of the PhC slabs. Individual densities are calculated using a CW plane wave excitation source with a frequency corresponding to the frequencies of respective transmission resonances (red curves) in Figs. 3(a-f), $g = 1.2a$ or $g = 1.0a$.
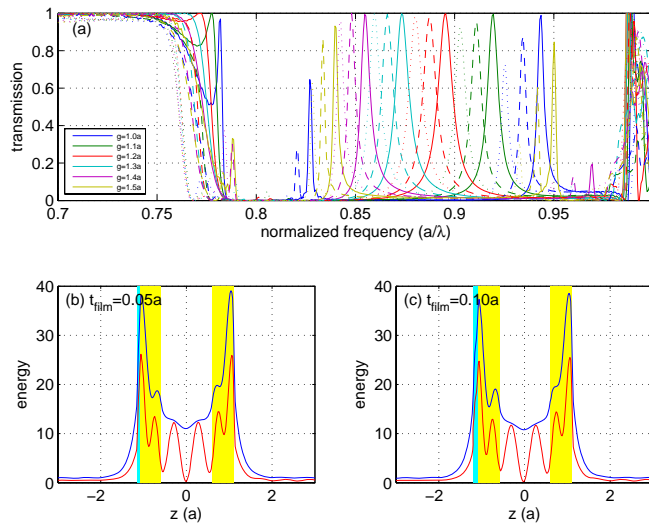

Fig. 6. (a) Transmissions of the structures of Fig. 5(c) (solid lines), with a $0.05a$ thick SiO_2 layer (dash lines) and a $0.10a$ thick SiO_2 layer (dot lines) for different gaps g. (b) and (c): same as Fig. 5(c) with respectively a $0.05a$ and $0.10a$ thick SiO_2 layer added (cyan area), at the frequencies of the red peaks of (a).
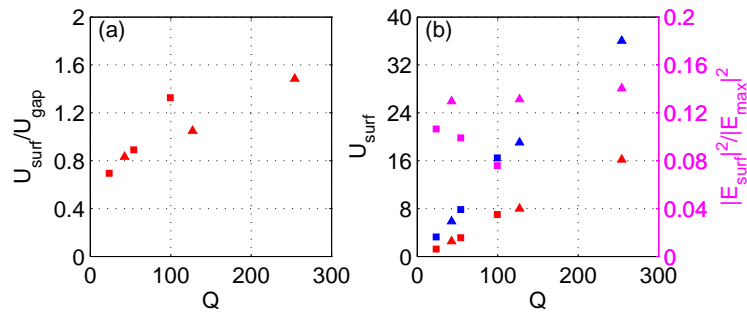
Fig. 7. (a) Ratio of linear electric energy density at the external surface of a PhC slab to the average linear electric energy density in the gap (U_{surf}/U_{gap}) vs. quality factor (Q) of the double layer PhC cavity system. (b) Linear energy density at the external surface of a PhC slab (U_{surf}) vs. quality factor (Q) – the red denotes the electric energy and the blue denotes the total energy – and electric field intensity at the external air/slab interface divided by maximum electric field intensity in the whole structure ($|E_{surf}|^2/|E_{max}|^2$, magenta). In all the plots, squares represent data for square lattice and triangles for triangular lattice.

slab PhC structure. In Fig. 7(b), we show the energy at the surface versus the quality factor. They follow roughly a proportional relation, which is not surprising since the energy stored in the resonator is proportional to its quality factor.

We also plotted the average electric field intensity at the external air/slab interface over the maximum electric field intensity in the whole structure (Fig. 7(b)). As previously, we took the air side value of the intensity with the same extrapolation. No strong correlation is found in relation with the quality factor, and values up to 0.14 are reached. Case (f) of Fig. 5 actually shows the best performance simultaneously in terms of U_{surf}, Q and $|E_{surf}|^2/|E_{max}|^2$.

These quantities, U_{surf}, Q and $|E_{surf}|^2/|E_{max}|^2$, displayed together in Fig. 7(b), represent the capabilities of enhancement of the structure. The capability of enhanced excitation is directly related to the electric energy density U_{surf} (normalized to the one in free space) at the surface where the QDs are, by having more light to be absorbed by them. The capability of enhanced emission is related to the quality factor (Q) through the Purcell factor[31] and to the ratio of fields square ($|E_{surf}|^2/|E_{max}|^2$), by maximizing the coupling of emitted light into the desired mode (global resonator mode – whom guided resonance is part of) and increasing the spontaneous emission rate of the QDs.[32–34] Enhanced excitation or emission can be performed depending on the parameters of the structure, and both can even be simultaneously performed by using two modes of the Fabry-Perot cavity, one at excitation wavelength, one at emission wavelength of the QDs. By example, the two magenta peaks of Fig. 3(f) could be used. Nevertheless, the appeal of our system is primarily for simultaneously enhancing and tuning the emission of QDs placed on the easy-access PhC surface.

Since the quality factor of our resonator is limited to a value around 250, scattering-induced losses due to fabrication quality limitations are expected to be negligible compared to the intrinsic losses of the resonator, and therefore are not expected to degrade the performances of the system.

4. Conclusions

Using the finite-difference time-domain method, we investigated tunable structures based on a two PhC slab geometry for their potential application in the enhancement of fluorescence emission. Individual PhC slabs consist of square or triangular lattices of cylindrical holes etched in

a silicon nitride layer. We demonstrate that the tuning of the narrow transmission resonance can be performed by changing the size of a gap between the two PhC slabs. As an example (Fig. 3(e)), a tunable range of 75 nm can be obtained for a 4 nm wide transmission peak in the operation range of $511 - 586$ nm. Finally, we demonstrate electrical field intensity enhancement with a factor 32 at the outer surface of a two slab PhC structure. This result is of direct utility for the design of high sensitivity fluorescence detection based biosensors.

Acknowlegements